JOURNAL OF SOLID STATE CHEMISTRY **129,** 165–173 (1997)
ARTICLE NO. SC967167

From Carbonate-Cuprates to Cuprate-Carbonates: The Structural Equivalence of CO_3 and CuO_x Groups in the Ba–Cu–C–O System

F. C. Matacotta,*[,1] G. Calestani,[‡,§] A. Migliori,[§] P. Nozar,[†,§] P. Scardi,[‖] O. Greco,* P. Ricci,* A. Tomasi,[¶] and K. A. Thomas**

*CNR-ISM, Area della Ricerca di Bologna, Via Gobetti, 101, 40129 Bologna, Italy; [†]ICTP, P.O. Box 586, 34100 Trieste, Italy; [‡]Dip. Chimica Fisica e Inorganica, Univ. di Bologna, 40136 Bologna, Italy; [§]CNR-LAMEL, Area della Ricerca di Bologna, 40129 Bologna, Italy; [‖]Dip. Ingegneria dei Materiali, Univ. di Trento, 38050 Trento, Italy; [¶]CMBM, 38050 Trento, Italy; and **CNR-CSSD, Università di Parma, 43100 Parma, Italy

Received May 24, 1996; in revised form September 18, 1996; accepted September 24, 1996

X-ray diffraction analysis of the phases forming from the decomposition of metastable double perovskites $Ba_2Cu_{1+x}(CO_3)_{1-x}O_{2+\delta}$ or by reacting $BaCO_3$, BaO_2, and CuO does not apparently reveal, or shows only traces of, copper containing compounds. The resulting diffraction patterns are very close to aragonite-like γ-$BaCO_3$. However, infrared and Raman spectroscopy data, electron diffraction, energy dispersion X-ray analysis performed on single crystal micrograins, and high-resolution electron microscopy reveal the existence of a mimetic compound corresponding to the formula $Ba(CuO_x)_{1-y}(CO_3)_y$, $y \leq 0.5$, with lattice constants practically identical to those of γ-$BaCO_3$. The new structure is characterized by the same hexagonal close packing of the Ba atoms, but the octahedral cavities are indifferently occupied by carbonate groups or CuO_x planar units, linked to form uniaxial chains. The length order in the $Ba(CuO_x)_{1-y}(CO_3)_y$ phase is extremely short reflecting the equal probability that a row of cavities is occupied by carbonate columns or CuO_x chains. Under suitable conditions, not completely identified as yet, the double perovskite and the aragonite-like structures transform one into the other on thermal cycling.

INTRODUCTION

The presence of carbonate groups in the layered cuprate structures is now considered a rather common fact. A great number of alkaline-earth copper oxycarbonates has been discovered in the past 7 years after the pioneering work of Müller-Buschbaum (1). The carbonate groups are found in the place of cuprate groups in many layered perovskite compounds, the prototype of which is $Sr_2CuO_2(CO_3)$ (2–4). When Sr is replaced by barium (5–7), several slight but important changes are induced in the structure and the chemical behavior of the resulting compounds is totally modified. In particular, these barium-based oxycarbonates can easily form in air from mixtures of pure BaO and CuO; it has been found that, at temperatures in excess of 850°C, these are able to efficiently intake the necessary CO_2 (8, 9). Furthermore, in these compounds the Cu/CO_3 ratio is found to vary continuously over a wide compositional range as a function of temperature and atmosphere giving rise to a series of slight structural modifications involving the CuO_x and CO_3 sublattice (9).

The carbonate group has also been found to substitute for cuprate groups at least in one nonperovskite compound, $BaCuO_2$, that has been long considered a pure oxide (10). Simultaneous neutron and X-ray diffraction refinements pointed out that this compound can take carbonate groups up to the composition $Ba_{44}Cu_{48}(CO_3)_6O_{88}$ and the presence of carbonate groups is most probably responsible for its previously reported nonstoichiometry in oxygen. Such discoveries should induce a deeper consideration of the system Ba–Cu–O as it seems that in this system the so far unsuspected affinity between carbonate and cuprate groups easily leads to the formation of oxycarbonates whenever the materials are exposed to carbon contamination.

Since the structural equivalence between the carbonate and cuprate groups manifests itself in a large number of barium-containing oxides, we have started to consider the inverse phenomenon, i.e., the possibility to incorporate cuprate groups in the barium carbonate structures. Our attention was originally attracted by the fact that, for low values of x, the perovskite-like $Ba_2Cu_{1+x}(CO_3)_{1-x}O_{2+\delta}$ compounds are metastable and decompose at about 400°C. According to XRD analysis the decomposition product mainly consists of $BaCO_3$, plus small amounts of copper-containing impurities. However, the color of the decomposed mixture is almost black, which, on a very qualitative approach, is not consistent with its apparent composition.

[1] To whom correspondence should be addressed.

0022-4596/97 $25.00

More quantitatively, the carbonate content of the decomposition products, measured by chemical analysis, was found to be about a factor of 2 lower than the value that could have been expected taking into account the XRD peak ratios.

The barium carbonate $BaCO_3$ has different crystalline forms, stable at different temperatures. Below 800°C, $BaCO_3$ has an aragonite-like structure (11, 12) (γ-$BaCO_3$, natural witherite, orthorhombic, space group *Pnma*, $a = 6.428$ Å, $b = 5.312$ Å, $c = 8.896$ Å) based on the hexagonal close packing of the Ba atoms, shown schematically in Fig. 1. The carbonate groups occupy the octahedral cavities forming columns aligned with the *a* axis. To match the Ba–O distances, the carbonates are rigidly lifted off the center of the octahedron producing a symmetry decrease from hexagonal to orthorhombic.

Even if there is no obvious way to exchange the carbonates with cuprates in this structure, the Ba–Ba distances involved are very close to the corresponding distances found in the carbonate-containing oxide structures. If the suitable size of the Ba sublattice is at the origin of the exchange between CuO_x and CO_3 groups in oxides, a similar effect should be possible in the carbonate structures.

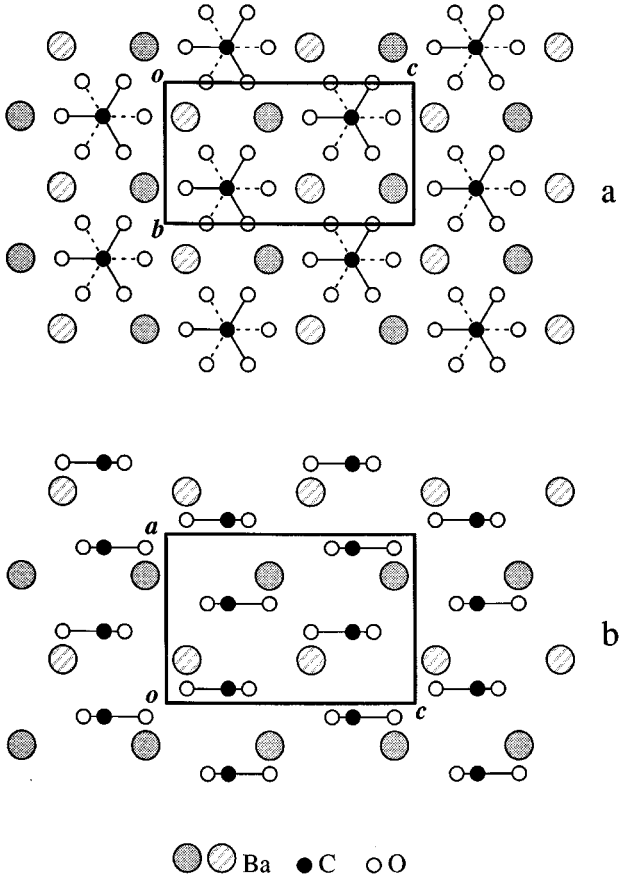

FIG. 1. Schematic view of the structure of γ-$BaCO_3$. (a) Projection onto the *bc* plane; (b) the same structure projected onto the *ac* plane. The differently shadowed barium atoms belong to different planes of the hexagonal stacking along the *a* axis.

EXPERIMENTAL

All samples have been prepared using 99.95% pure CuO, 99.98% pure $BaCO_3$, and 98% pure BaO_2. Our analysis showed that the barium peroxide powders typically contained 2% (molar) $BaCO_3$ and its cation purity was certainly above 99.8%. The samples under study were prepared using different processes:

(a) formation of the perovskite-like barium copper oxycarbonate $Ba_2Cu_{1.2}(CO_3)_{0.8}O_{2+\delta}$ at 900°C and decomposition of the same in air or flowing oxygen at $T > 380$°C (method a).

(b) solid state reaction of $BaCO_3$, BaO_2, and CuO in different proportions (Ba/Cu ratio ranging from 4 : 1 to 4 : 2; CO_3/Cu > 1), in air or flowing oxygen at $T > 600$°C (method b).

The total carbonate content of the starting materials and of the resulting samples has been estimated by absorbing on fresh ascarite the CO_2 fraction of the gas evolved during the decomposition of the samples in concentrated H_3PO_4.

The reacted materials have been analyzed by standard X-ray powder diffraction (XRD) using Cu$K\alpha$ radiation with an automated Philips PW1050 powder diffractometer. Formation/decomposition kinetics have been monitored by high temperature XRD using a Rigaku III D-max diffractometer (Cu$K\alpha$ radiation) equipped with a high-temperature sample holder in which, in order to avoid any contamination from furnace materials, the samples were protected with gold foil. Differential scanning calorimetry (DSC) under various atmospheres up to 600°C was performed using a Perkin–Elmer series 7 automatic system. Mid- and far-infrared absorption spectra have been measured using a Bruker IFS 113 Fourier transform spectrometer and KBr- and CsI-pellet methods, respectively. Fourier transform Raman spectra (backscattering mode) have been collected exciting the samples at 1.16 eV with a beam power of less than 40 mW and a beam diameter of 0.1 mm using a Bruker RFS 100 Raman spectrometer.

Selected area electron diffraction (SAED) and high-resolution electron microscopy (HREM) have been carried out using a Philips CM300 transmission microscope operating at 300 kV equipped with energy dispersion X-ray microanalysis (EDX). To prepare the samples, the as prepared materials were mildly ground in an agate mortar with 2-propanol and the resulting powders were spread on perforated carbon films supported by Ti grids.

RESULTS

XRD patterns taken at increasing temperatures during a *fast* heating ramp (ramp rate 30°C/min) in dry air from a pelletized sample of $Ba_2Cu_{1.2}(CO_3)_{0.8}O_{2+\delta}$ are shown in Fig. 2. In order to decrease the temperature difference between the start and end point of each diffraction scan and between subsequent scans, the 2θ range has been limited to a region (21°–32°) where the most dramatic intensity changes occur. It is evident that between 417 and 447°C the double perovskite structure is lost and a new pattern, very similar to that of γ-$BaCO_3$, appears. The transformation is completed in about 4 min. A set of XRD experiments taken at different temperatures under isothermal conditions on a mixture of $BaCO_3$, BaO_2, and CuO (in the proportions 3 : 1 : 1) resulted in the XRD patterns shown in Fig. 3. Again, above 500°C, the majority phase seems to be γ-$BaCO_3$. In this case, the transformation was slower and was completed only when the temperature was close to 600°C. In both series of experiments, only very weak traces of CuO or other known Cu-containing impurities are detected.

DSC experiments were performed on $BaCO_3$, BaO_2, and CuO mixtures under similar conditions. They have evidenced the existence of strong endothermic feature peaked at 430°C (Fig. 4). Such a feature is only found when all the three compounds are present and is maximum when the mixture proportions are close to 3 : 1 : 1. More details on these experiments are given in a different paper (13).

The room temperature powder XRD patterns of the materials obtained using the processes described in the previous section are very similar and reveal the presence of a main phase with a diffraction pattern almost exactly corresponding to γ-$BaCO_3$. Weak or very weak peaks corresponding to CuO, $BaCuO_2$, and $Ba_2Cu_3O_{5+\delta}$ (14) are found.

Qualitatively, the intensity analysis of the XRD patterns indicates that the amount of crystalline copper-containing impurities is much less than to what should be expected from the starting Ba : Cu contents.

Furthermore, the reaction products are much darker (from dark brownish grey to black) than what should be expected from the mixtures of $BaCO_3$ and copper-containing impurities resulting from a straightforward

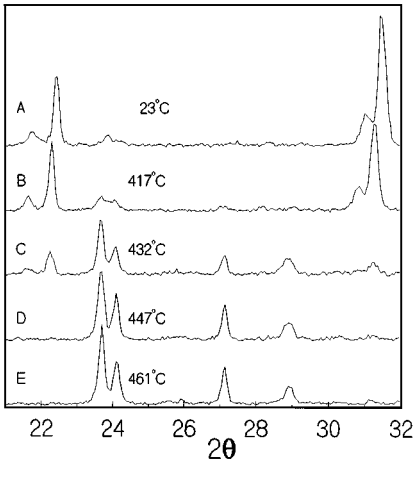

FIG. 2. Powder XRD patterns (scan rate 1°/sec, scan width 11°) taken in dry air during a fast heating ramp (+30°C/min) from a pellet of $Ba_2Cu_{1.2}(CO_3)_{0.8}O_2$. Comparing the intensities of the 100/002 reflections at about 22° and 110/102 doublet at about 31° in curves A and C, it is possible to estimate the velocity of the transformation of the double perovskite to an aragonite-like phase.

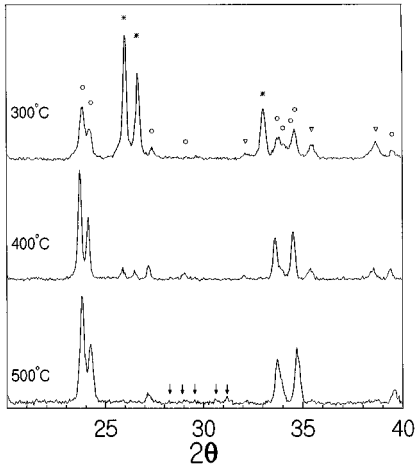

FIG. 3. Powder XRD patterns taken isothermally in dry air at different temperatures from a pellet of $BaCO_3$ (open circles), BaO_2 (asterisks), and CuO (inverse triangles) mixed in the proportions 3 : 1 : 1. Arrows in bottom curve indicate the position of various Cu-containing impurity phases.

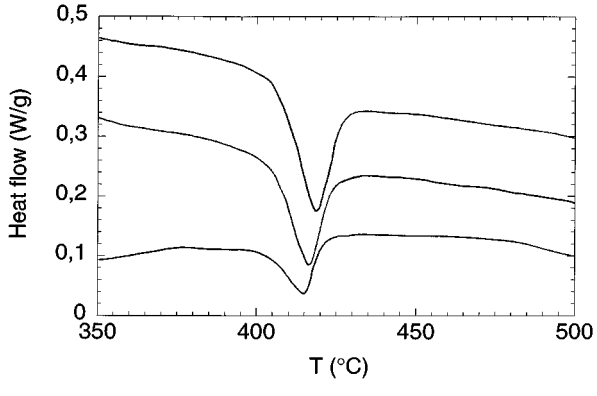

FIG. 4. DSC curves taken from a mixture of $BaCO_3$, BaO_2, and CuO (in 3 : 1 : 1 proportions) in dry air at different heating rates. From top to bottom: 50, 40, and 10°C/min. The experimental setup is such that esothermal and endothermal processes give rise to upward or downward features, respectively.

interpretation of the corresponding XRD patterns (for clarity purposes only, in the following we shall refer to these materials as "black $BaCO_3$"). Indeed, a detailed analysis of their XRD patterns reveals some slight reproducible differences with respect to the typical patterns of γ-$BaCO_3$. In particular, the c lattice parameter decreases systematically (0.3%), one order of magnitude above the typical fluctuation found in different samples of γ-$BaCO_3$. Moreover, in the presence of copper sources, the line profiles of the diffraction peaks become broader in spite of the thermal treatments, indicating a decrease of the crystallinity.

Typical infrared absorption and Raman spectra of black $BaCO_3$ and pure $BaCO_3$ are shown in Fig. 5. The most striking feature in all the spectra of the black $BaCO_3$ is the presence of modes, both in IR and Raman, in the spectral region where the Cu–O vibrations are found (15–17). Their intensity ratios are constant in all the investigated samples. A list of the frequencies of these modes is given in Table 1. The frequencies of intense IR and Raman modes of the possible impurity phases (γ-$BaCO_3$, CuO, $BaCuO_2$, $Ba_2Cu_3O_{5+\delta}$, $Ba_2Cu_{1+x}(CO_3)_{1-x}O_{2+\delta}$) are listed in the same table for comparison. The series of frequencies of the

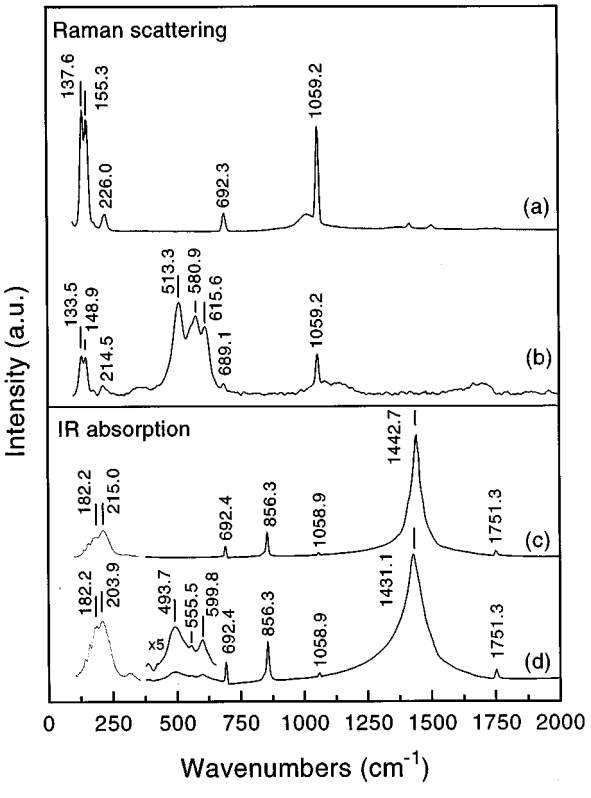

FIG. 5. Fourier transform Raman spectra of (a) pure γ-$BaCO_3$ and (b) black $BaCO_3$. IR absorption spectra of (c) pure γ-$BaCO_3$ and (d) black $BaCO_3$. The IR region of the Cu–O phonons has been reproduced with intensity originally magnified by a factor 5. The frequencies of the most intense and characteristic phonons are indicated.

TABLE 1

IR and Raman Vibration Frequencies for Black $BaCO_3$, γ-$BaCO_3$, and Copper-Containing Compounds That Are Likely to Be Present as Impurities in the Examined Samples

Black $BaCO_3$	$BaCO_3$	CuO	IR $BaCuO_2$	$Ba_2Cu_3O_{5+\delta}$	$Ba_2Cu_{1.2}(CO_3)_{0.8}O_{2+\delta}$
182.2	182.2		289.9	245.9	174.5
203.9	**215.0**				257.3
315.4		319.0	314.0	304.6	319.6
				329.6	
383.7		413.2	391.0		378.5
			472.6	445.5	449.1
493.7		504.9		505.4	500.5
555.5			538.9	537.7	
599.8		605.1	613.6	602.3	
641.2			669.6		
692.4	692.4				692.5
856.3	856.3				862.9
1058.9	1058.9				1060.9
1431.1	**1442.7**				1430.2
Black $BaCO_3$	**$BaCO_3$**	**CuO**	**RAMAN $BaCuO_2$**	**$Ba_2Cu_3O_{5+\delta}$**	**$Ba_2Cu_{1.2}(CO_3)_{0.8}O_{2+\delta}$**
133.5	**137.6**				
148.9	**155.3**				
214.5	**226.0**				
		347.4			
				456.1	464.2
513.3			512.9	517.6	499.5
		524.7	530.7		536.0
580.9		581.4	574.7	564.0	583.6
615.6		628.1		630.1	
689.1	692.3				
1059.2	1059.2				1060.3

Numbers in bold indicate the most significant shifts detected, as discussed in the text.

black $BaCO_3$ in the Cu–O vibration range do not correspond to any known Cu-containing impurity phases. Comparing the spectra of black $BaCO_3$ and γ-$BaCO_3$ in Fig. 5 and Table 1, the changes in the low-energy modes, assigned to vibrations involving barium atoms, are interesting as they reveal that the barium environment has the same symmetry but is definitely modified in the black $BaCO_3$. Very few changes are shown by the free carbonate phonons at higher energies. Only the IR mode at 1440 cm^{-1} is shifted; this mode is related to the E' vibration of the free carbonate group. However, the shift exhibited by the IR phonon (-11.6 wavenumbers) could be due to spurious effects related to the increased reflection contributions, as indicated by the broadening of the band.

So far, all experiments gave evidence that an unexpected phenomenon takes place in different systems containing

Ba, Cu, and the carbonate ion in the temperature range 400–650°C. The XRD analysis gives ambiguous results as it does not reveal the formation of a new copper-containing phase but only an indication of changes involving microstructure and grain size of γ-$BaCO_3$. In contrast, optical spectroscopies indicate the appearance of a new phase characterized by a typical series of copper–oxygen vibrations that are not found in known compounds of the system Ba–Cu–C–O.

Transmission electron microscopy techniques (EDX analysis, SAED, HREM) give the most convincing proof that the black $BaCO_3$ is a copper-containing compound having almost the same structure of γ-$BaCO_3$. EDX analyses, performed on a large number of grains, revealed for each crystallite a copper content of no less than 0.2 atoms per atom of barium (with a maximum of 0.5 found in a few grains). The measured copper content is by far too large to be attributed to impurity surface layers or inclusions. At the same time SAED patterns taken from the same areas revealed a close similitude with those of γ-$BaCO_3$. However, electron diffraction patterns show the appearance of weak reflections, some of which are forbidden by symmetry, as shown in Fig. 6 where the SAED pattern taken along the $\langle 110 \rangle$ projection for a grain, showing a Cu to Ba ratio of 0.25, is compared to a similar pattern taken from a γ-$BaCO_3$ grain. Spots corresponding to the forbidden $00l$, $l = 2n + 1$ reflections are clearly present, indicating either a breaking of the symmetry or doubling of the c axis. On the other hand such an effect could be due to the very peculiar twinning domain structure evidenced by high-resolution studies in both copper-containing grains and, to a less extent, in pure $BaCO_3$. HREM images showed that all the grains consist of domains with a typical size of some tens of nanometers, which are tilted 120° in the bc plane. This phenomenon derives from the pseudo-hexagonal character of the aragonite structure and is typically observed in γ-$BaCO_3$. In Fig. 7 two typical high-resolution images of the bc plane of pure γ-$BaCO_3$ (Fig. 7a) and black $BaCO_3$ (Fig. 7b) are compared.

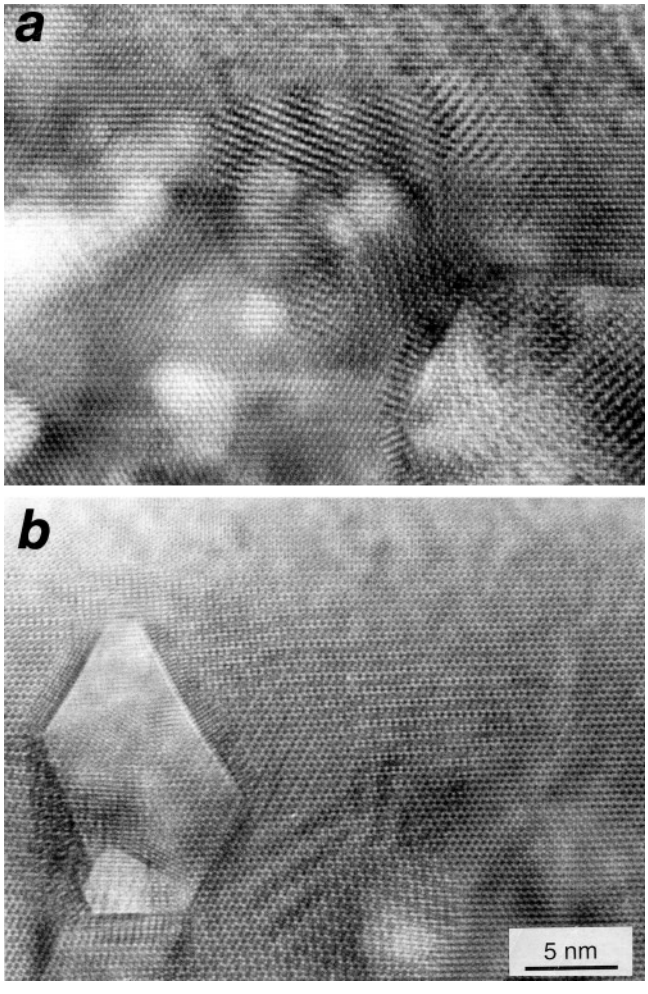

FIG. 7. (a) Low-magnification HREM image taken along the $\langle 100 \rangle$ direction of a typical portion of a thin γ-$BaCO_3$ grain. The domain structure with 120° boundaries is well evidenced; (b) Low-magnification HREM image of a thin portion of a typical black $BaCO_3$ grain taken along $\langle 100 \rangle$ showing again a dense domain structure. Some domains are characterized by rows with different contrast mutually stacked in various ways in the bc plane.

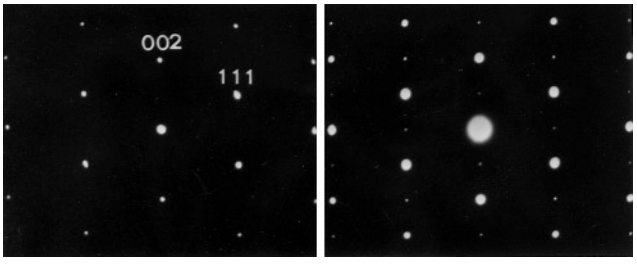

FIG. 6. Typical SAED images, taken along the $\langle 110 \rangle$ direction and under the same conditions, from (a) a grain of γ-$BaCO_3$ and (b) a grain of black $BaCO_3$. The extreme similarity of the two structures is evident. However, among the weak extra spots present in image (B) those corresponding to $00l$, $l = 2n + 1$; $hk0$, $h = 2n + 1$, are forbidden by the *Pnma* symmetry of γ- $BaCO_3$.

All the HREM images of the black $BaCO_3$ evidenced features that cannot be explained in terms of the $BaCO_3$ structure, but require the presence of different atoms on almost equivalent sites of the lattice. In particular, the images taken along (100) evidenced (Fig. 7b) two types of rows of dots with different contrast, always aligned with one of the three possible equivalent directions of the pseudo-hexagonal bc plane and mutually stacked in several ways in the plane. These contrast patterns, never found in γ-$BaCO_3$, suggest, consistently with the information obtained from all the different techniques we have used, an interpretation in terms of substitution of some carbonate columns (aligned with the a axis of the aragonite-like structure) with copper–oxygen linear substructures. This hypothesis was

confirmed by HREM images taken in directions perpendicular to the stacking axis. Unfortunately, no detailed information on the relative arrangement of the CuO_x groups was obtained, since the high degree of disorder in the CO_3–CuO_x sequences in the *bc* plane produces random superimposition when looking perpendicularly to the *a* axis.

Starting from the hypothesis that the contrast patterns observed in the HREM images of the black $BaCO_3$ should be considered as the signature of CuO_x groups (linked to form unidimensional chains perpendicular to the *bc* plane) replacing some carbonate columns, several structural models have been formulated to describe the copper-containing barium carbonate. All the models involve Cu atoms at the center of octahedral cavities, formed by Ba atoms, from which the carbonates are removed. This site represents the most suitable choice for a copper atom in the barium sublattice, in analogy with the structure of $BaNiO_3$ and corresponds to Ba–Cu distances of order 3.5 Å, a value which is typically observed in the barium cuprates.

Preliminary simulations of the HREM images have been performed by considering a large aragonite supercell ($a \times b \times 10c$), in which one half of carbonate columns are removed and replaced in an ordered way by copper atoms columns, in order to verify if this substitution is at the origin of the peculiar contrast features of black $BaCO_3$. In this first step the contribution of the oxygen atoms surrounding Cu was neglected. Figure 8 shows the comparison of a simulated and an experimental HREM image taken along the *a* axis and provides a further confirmation on the origin of the contrast features. The localization of the oxygen atoms of the CuO_x groups represents a more difficult problem. By considering the usual Ba–O and Cu–O bond distances and the typical coordinations presented by Ba and Cu in their compounds and by taking into account the linking of the CuO_x groups in unidimensional chains, several hypothesis, which differ for the number and the geometry of the oxygen atoms of the CuO_x group, can be advanced. In theory it is possible to vary the nature of the unidimensional linking along *a* of the CuO_x groups from simple zigzag chains of CuO_2 dumbbells, to zigzag chains of planar CuO_4 units sharing corners or edges, to more complex arrangements involving simultaneously squares, square pyramids, and octahedra.

Among the possible structural models, the one used for HREM simulation, involving zigzag chains of planar CuO_4 units, obtained by considering an idealized ordering of cuprate and carbonate groups in 1 : 1 ratio in the

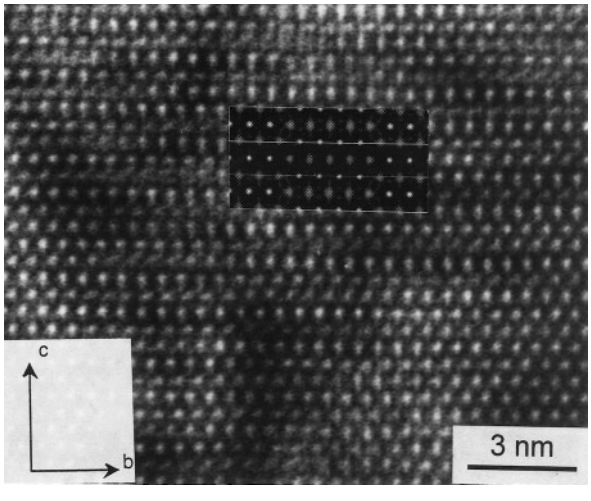

FIG. 8. HREM image taken along the ⟨100⟩ direction of a thin black $BaCO_3$ grain. A simulated pattern (defocus −90 nm, thickness 26 nm), generated using an ordered $a \times b \times 10c$ supercell, is inserted. In the simulated image, bright spots correspond to carbonate columns perpendicular to the *bc* plane, whereas diffuse spots correspond to copper columns.

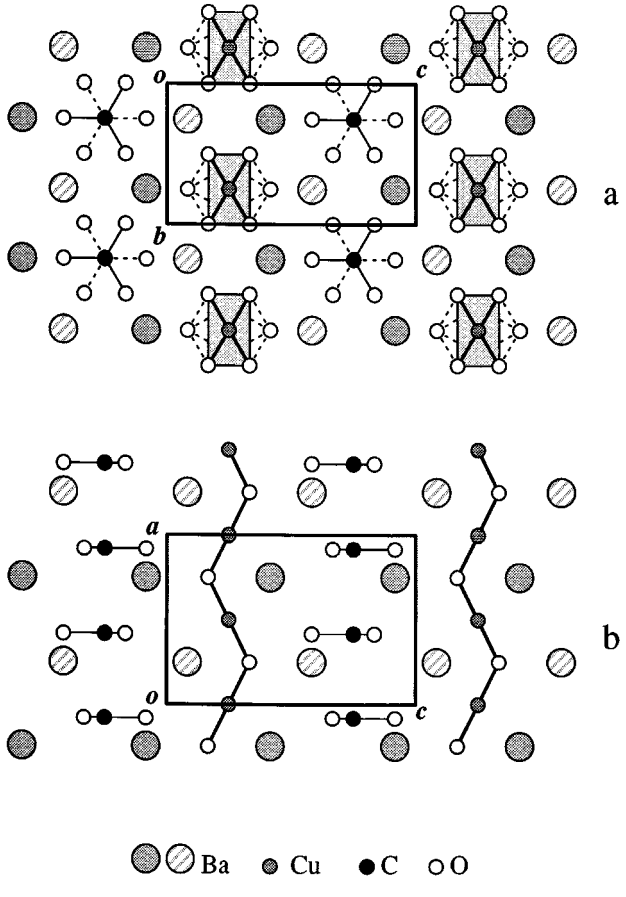

FIG. 9. Schematic view of the ordered structural model utilized for the simulation of the HREM images of the copper containing compound: (a) projection onto the *bc* plane. The three possible orientations of the CuO_4 planar groups with respect to the hexagonal barium sublattice are indicated. (b) The same model, projection onto the *ac* plane. For simplicity, only one of the possible orientations for the CuO_4 groups (the one shaded in (a)) is shown.

noncentrosymmetric space group $P2_1ma$, is schematically shown in Fig. 9. Figure 10 shows an enlarged region of an observed HREM image compared with two simulated images obtained from the pure $BaCO_3$ structure and from the ordered model of the copper-containing aragonite structure shown in Fig. 9. Both simulations fit well different regions of the experimental image showing that the copper content found by EDX results from averaging different local situations that range from pure $BaCO_3$ to heavily substituted $Ba(CuO_x)_{1-y}(CO_3)_y$. The cuprate inclusions are not spread in the whole materials but tend to condense in regions for which y tends to 0.5.

The HREM images show that, in the heavily substituted regions, the carbonate and cuprate columns tend to order one to one in the bc plane creating alternate rows running along the three possible twinning directions deriving from the pseudo-hexagonal character of the aragonite so that the twinning density increases. Moreover, the ordering extends over a short range: along the same row in the bc plane a carbonate sequence is replaced after a few nanometers by a cuprate sequence and so on, creating a huge number of local order possibilities. Under these conditions, in which large regions of nonperturbed γ-$BaCO_3$ are associated with small $Ba(CuO_x)_{1-y}(CO_3)_y$ domains, powder XRD experiments cannot provide a clear evidence of the phenomenon, but give an indication of the decrease of the grain size which is connected with the increase of twinning density. Moreover, it is interesting to note that the calculated XRD pattern, generated starting from the ordered model we used to simulate the HREM images of $Ba(CuO_x)_{1-y}(CO_3)_y$, do not differ too much from a typical γ-$BaCO_3$ pattern, the main differences consisting in the presence of a few weak reflections and in slight changes of the relative intensities (Fig. 11). The lack of diffraction information prevents one from not only carrying out deeper structural characterization but even assigning definitively, among the different developed models, the most probable CuO_x unit that occurs in the cuprate linking.

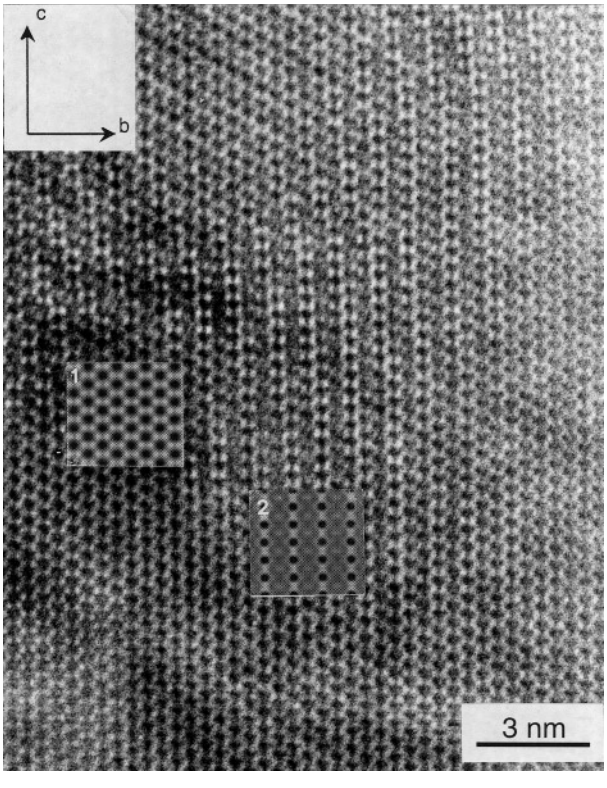

FIG. 10. Enlarged image of the area shown in Fig. 7b compared with simulated images (defocus -77 nm, thickness ≈ 13 nm) of γ-$BaCO_3$ (1) and of the model structure $Ba(CuO_x)_{1/2}(CO_3)_{1/2}$ (2). On the basis of the simulated images contrast patterns, the black circles surrounded by annular grey regions represent carbonate groups whereas the sandwiched lower contrast rows are produced by cuprate groups.

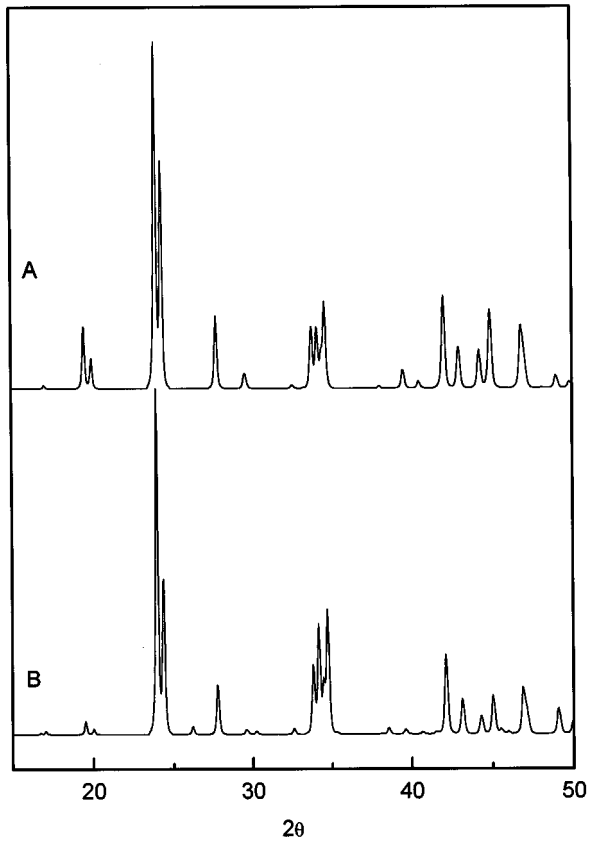

FIG. 11. XRD pattern simulations generated using the $Pnma$ unit cell of γ-$BaCO_3$ (A) and the $P2_1$ ma model unit cell of $Ba(CuO_2)_{0.5}(CO_3)_{0.5}$ (B). The lattice constants used result from the average of different experimental refinements. A part from the changes of spacing and intensity of some peaks, partly due to the slight shift of the cell parameters, a series of extra reflections appears in the $P2_1ma$ pattern. However, the intensity of these reflections is always comparable with the typical experimental noise.

Heating the copper-containing carbonate phase above 800°C, two distinct behaviors appear, independent of process parameters like temperature ramp rates or atmosphere composition. High-temperature powder XRD experiments may show a transformation of the aragonite-like structure in the double perovskite structure similar to $Sr_2CuO_2(CO_3)$ or in a phase very similar to the calcite-like high-temperature modification of $BaCO_3$ (Fig. 12) (12). At present, we have no experimental proof that the calcite-like phase does contain copper. This phase is not quenchable and we could not perform any significant high-temperature experiment to determine the presence of copper in this structure. However, since samples of the same batch of $Ba(CuO_x)_{1-y}(CO_3)_y$ resulted in the copper-containing perovskite-like phase, it is likely that also in the calcite-like structure the substitution of carbonate groups by CuO_x blocks takes place to some extent. Both the calcite-like modification of $BaCO_3$ and the double perovskite structures are characterized by cubic close packing of barium atoms. A projection of the calcite structure is compared in Fig. 13 with a hypothetical model of a calcite-like phase containing distorted CuO_2 planes and with the double perovskite structure of $Ba(CuO_x)_{1-y}(CO_3)_y$. The differences between the two copper-containing structures are not pronounced and one can be generated by the other by a simple displacive transition. In a speculative way, the nonunique evolution of the new phase at high temperatures would reflect the existence of different prevailing orderings in the copper–carbon–oxygen sublattice of the aragonite-like structure which, in the aragonite–calcite phase transition, can produce one- or two-dimensional linking of CuO_4 units. Whereas the bidimensional linking (CuO_2 planes) is expected to produce an immediate transition to the perovskite structure, an unidimensional arrangement could survive in a calcite-like structure.

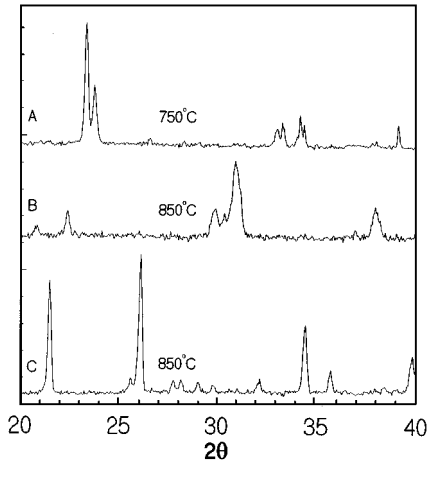

FIG. 12. Powder XRD patterns taken at fixed temperatures in dry air from two pellets made from the same 3 : 1 : 1 mixture of $BaCO_3$, BaO_2, and CuO. The patterns taken at 750°C were almost identical (one is not shown). At 850°C, one pellet shows the typical pattern of the double perovskite phase $Ba_2Cu_{1+x}(CO_3)_{1-x}O_{2+\delta}$ (curve B); the other one shows a pattern indexable with the rhombohedral unit cell of high temperature calcite-like modification of $BaCO_3$ (curve C).

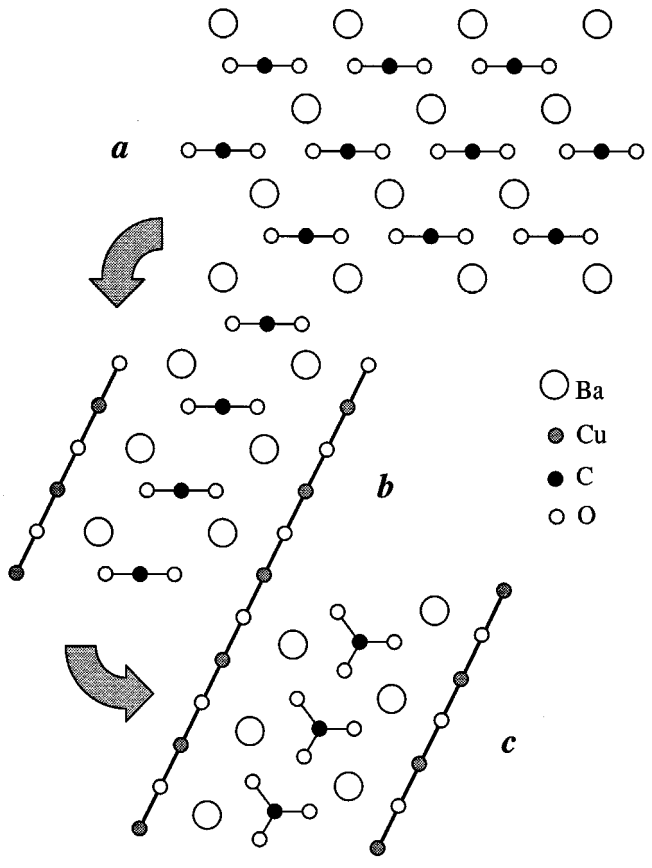

FIG. 13. Schematic views of: (a) the 110 plane (in the hexagonal description) of the distorted NaCl structure of the rhombohedral (calcite) high temperature modification of $BaCO_3$; (b) the corresponding plane derived from an ordered model for a hypothetical copper containing calcite-like $Ba(CuO_x)_{1/2}(CO_3)_{1/2}$ compound; (c) the *ac* plane of the double perovskite structure of $Ba_2Cu_{1+x}(CO_3)_{1-x}O_2$ (for simplicity, $x = 0$).

DISCUSSION AND CONCLUSIONS

In 1989, the discovery of the first oxycarbonate of strontium and copper with a double perovskite structure, resulting from the alternate stacking of CuO_2 and carbonate layers, was considered an unexpected result. Since then several similar structures with strontium or barium have been described and a few of then now have an important impact in the field of high-T_c materials as they are, so far, the only superconductors with T_c in excess of 100 K not containing toxic heavy metals (18, 19). These compounds have been frequently defined as "carbocuprates" (carbonate–cuprates) indicating with this non-IUPAC term the fact

that, despite the presence of large amounts of carbonate ions, their structure preserves the typical features of the cuprate compounds. Recently, we have found that in layered barium "carbocuprates," the relative content of Cu and C in the carbonate layer varies reversibly over a wide range as a continuous function of temperature and partial CO_2 pressure (9). The variations in the stoichiometry produce significant changes in the structure. By decreasing the carbonate content the structure loses its layered character and by successive ordering involving carbonate and cuprate groups it becomes more and more tridimensional.

In the present paper we report on a series of experiments pointing out the existence of a surprisingly mimetic copper-containing phase, whose structure is strictly related to the γ-$BaCO_3$ aragonite-type phase. The unit cell parameters do not differ for more than 0.3%. The new phase contains large amounts of copper, replacing carbonate groups, ordered over very short range. The recognition and description of the new phase has posed interesting experimental problems because, due to the similarity between its structure and γ-$BaCO_3$ and the short order range, the usual diffraction techniques are not able to discriminate the contribution of the copper-containing compound. As a consequence, the structural information we present is only qualitative, but contains enough elements to appreciate the very unusual features of the copper-containing barium carbonate.

Under particular conditions, the aragonite-like and perovskite-like phases transform one into the other as a function of temperature. This finding allows us to express all the barium copper oxycarbonates by the chemical formula $Ba(CuO_x)_{1-y}(CO_3)_y$ indicating a "solid solution" involving carbonate and cuprate anions. However, this is true only on a macroscopic scale; the structural sequences are always ordered at least on a local scale due to the remarkable difference of size and geometry of the anions. According to the prevailing anion, the structure of $Ba(CuO_x)_{1-y}(CO_3)_y$ resembles the barium carbonate or barium copper oxides providing a rare example of structural mimicry which extends on different structures. This fact should induce a careful reconsideration of many results obtained in compounds of the Ba–Cu–O system, not only in all cases where they have been prepared from carbonate precursors, but also whenever they have been exposed to minimal CO_2 contamination. For instance, according to the present results, in many cases the barium carbonate phase that is found to be in equilibrium with the 123 or Tl-based superconductors should be $Ba(CuO_x)_{1-y}(CO_3)_y$ rather than $BaCO_3$.

The structural equivalence between two complex anions, the carbonate CO_3 and the cuprate CuO_x, different in dimensions, geometry, and (possibly) in charge, seems to be a rule in the barium compounds. From this standpoint, these compounds should be considered a new class for which the usual definition of oxycarbonates is not adequate since their variations of stoichiometry involve the substitution and the structural exchange of the entire cuprate and carbonate anionic groups. We therefore propose to define these compounds as carbonate–cuprates (carbocuprates) and cuprate–carbonates (cuprocarbonates) according to the prevailing oxyanion and the resulting character (oxide or carbonate) of the structure. On the basis of our results the cuprocarbonate and the carbocuprate could be considered the low- and high-temperature phase, respectively, in a system which is able to exchange CO_2 with the atmosphere as a function of the temperature varying in an almost continuous way the composition in two structures which seems to be related by a transition occurring around $y = 0.5$. This picture could be modified and complicated by the confirmation of the existence of a nonquenchable copper-containing calcite-like structure.

REFERENCES

1. Hk. Müller-Buschbaum, *Angew. Chem. Int. Ed. Engl.* **28,** 1472 (1989).
2. D. V. Fomichev, A. L. Kharlanov, E. V. Antipov, and L. M. Kovba, *Superconductivity* **3,** S126 (1990).
3. C. Chaillout, Q. Huang, R. J. Cava, J. Chenavas, A. Santoro, P. Bordet, J. L. Hodeau, J. J. Krajewski, J. P. Levy, M. Marezio, and W. F. Peck Jr., *Physica C* **195,** 335 (1992).
4. Y. Miyazaki, H. Yamane, N. Ohnishi, T. Kajitani, K. Hiraga, Y. Morii, S. Funahashi, and T. Hirai, *Physica C* **198,** 7 (1992).
5. F. C. Matacotta, D. Pal. T. Mertelj, P. Stastny, P. Nozar, D. Mateev, and P. Ganguly, *Solid State Commun.* **84,** 781 (1992).
6. A. R. Armstrong, H. S. Obhi, and P. P. Edwards, *J. Solid State Chem.* **106,** 120 (1993).
7. P. Ganguly, N. Shah, and F. C. Matacotta, *Physica C* **206,** 70 (1993)
8. M. Kikuchi, F. Izumi, M. Kikuchi, E. Ohshima, Y. Morii, Y. Shimoio, and Y. Syono, *Physica C* **247,** 183 (1995).
9. G. Calestani, F. C. Matacotta, A. Migliori, P. Nozar, L. Righi, and K. A. Thomas, *Physica C* **261,** 182 (1996).
10. M. A. G. Aranda and J. P. Attfield, *Angew. Chem. Int. Ed. Engl.* **32,** 1454 (1993).
11. R. W. G. Wyckoff, "Crystal Structures, 2nd Edition, Volume 2: Inorganic Compounds RX_n, R_nMX_2, R_nMX_3," p. 367. Interscience, New York, 1964.
12. Landolt-Börnstein, "Numerical Data and Functional Relationships in Science and Technology, Group III, Volume 7: Crystal Structure Data of Inorganic Compounds" (K.-H. Hellwege and A. M. Hellwege, Eds.), part C3, p. 110. Springer-Verlag, Berlin/Heidelberg/New York, 1979, and references therein.
13. A. Tomasi, P. Scardi, F. C. Matacotta, and P. Nozar, *J. Thermal Anal.* **47,** 27 (1996).
14. W. Wong-Ng and L. P. Cook, *Powder Diff.* **9,** 280 (1994) and references therein.
15. I. Genzel, A. Wittlin, M. Bauer, M. Cardona, E. Schonherr, and A. Simon, *Phys. Rev.* **B40,** 2170 (1989).
16. C. Infante, M. K. El-Mously, R. Dayal, M. Husain, S. A. Siddiqi, and P. Ganguly, *Physica C* **167,** 640 (1990).
17. T. Mertelj, D. Mateev, F. C. Matacotta, D. Pal, P. Stastny, P. Nozar, Q. D. Jiang, D. Mihailovic, and P. Ganguly, *Solid State Commun.* **84,** 1115 (1992).
18. T. Kawashima, Y. Matsui, and E. Takayama-Muromachi, *Physica C* **224,** 69 (1994).
19. D. Pelloquin, M. Herview, C. Michel, A. Maignan, and B. Raveau, *Physica C* **227,** 215 (1994).